



1           **Past Ocean surface density from planktonic foraminifera calcite  $\delta^{18}\text{O}$**

2

3   Thibaut Caley<sup>1</sup>, Niclas Rieger<sup>2,3</sup>, Martin Werner<sup>4</sup>, Claire Waelbroeck<sup>5</sup>, H  loise Barathieu<sup>1</sup>,  
4   Tamara Happ  <sup>6</sup>, Didier M. Roche<sup>7,8</sup>

5   1) Univ. Bordeaux, CNRS, Bordeaux INP, EPOC, UMR 5805, 33600 Pessac, France

6   2) Institut de Ci  ncies del Mar (ICM) - CSIC, Pg. Mar  tim de la Barceloneta 37, Barcelona, Spain

7   3) Centre de Recerca Matem  tica (CRM), Departament de F  sica, Bellaterra, Spain

8   4) Alfred Wegener Institute Helmholtz Centre for Polar and Marine Research, Bremerhaven, Germany

9   5) LOCEAN-IPSL, CNRS, Sorbonne Universit  , Paris, France

10   6) Institute for Environmental Studies, Vrije Universiteit Amsterdam, Amsterdam, The Netherlands

11   7) Laboratoire des Sciences du Climat et de l'Environnement, LSCE/IPSL, CEA-CNRS-UVSQ, Universit   Paris-  
12   Saclay, 91191 Gif-sur-Yvette, France

13   8) Earth and Climate Cluster, Faculty of Earth and Life Sciences, Vrije Universiteit Amsterdam, Amsterdam, the  
14   Netherlands

15

16

17

18

19   Correspondence to: Thibaut Caley ([thibaut.caley@u-bordeaux.fr](mailto:thibaut.caley@u-bordeaux.fr))

20

21

22

23

24

25

26

27

28

29

30

31

32



33 **Abstract**

34 Density of seawater is a critical property that controls ocean dynamics. Previous works  
35 suggest the use of the  $\delta^{18}\text{O}$  calcite of foraminifera as a potential proxy for paleodensity.  
36 However, potential quantitative reconstructions were limited to the tropical and subtropical  
37 surface ocean and without an explicit estimate of the uncertainty in calibration model  
38 parameters. We developed the use of the  $\delta^{18}\text{O}_{\text{c}}$  of planktonic foraminifera as a surface  
39 paleodensity proxy for the whole ocean using Bayesian regression models calibrated to  
40 annual surface density. Predictive performance of the models improves when we account  
41 for inter-species specific differences.

42 We investigate the additional uncertainties that could be introduced by potential evolution  
43 of the  $\delta^{18}\text{O}_{\text{c}}$ -density relationship with time (from the last glacial maximum (LGM) to the  
44 preindustrial (PI)) through the combination of past isotope enabled climate model  
45 simulations and a foraminiferal growth module. We demonstrate that additional  
46 uncertainties are weak globally, except for the Nordic Seas region.

47 We applied our Bayesian regression model to LGM and Late Holocene (LH)  $\delta^{18}\text{O}_{\text{c}}$   
48 foraminifera databases to reconstruct annual surface density during these periods. We  
49 observe stronger LGM density value changes at low latitudes compared to mid latitudes.  
50 These results will be used to evaluate numerical climate models in their ability to simulate  
51 ocean surface density during the extreme climatic period of the LGM.

52 The new calibration has great potential to be applied to other past periods and to  
53 reconstruct the past temporal evolution of ocean surface density.

54

55

56

57

58

59

60

61

62

63

64

65

66

67



68      1. Introduction

69      Temperature and salinity control the density of seawater and therefore the ocean dynamics  
70      too. Reconstruction of past ocean surface temperature with reasonable uncertainties is  
71      possible (MARGO, 2009; Tierney et al., 2020b) but reconstructions of past surface salinity  
72      remain very challenging in paleoceanography. When the current uncertainties on past  
73      temperature and salinity reconstructions are cumulated, it becomes unreasonable to  
74      combine these two parameters in order to quantify past ocean density and the past ocean  
75      dynamics.

76      Rather than using the combination of temperature and salinity, previous works suggest the  
77      use of the  $\delta^{18}\text{O}$  of foraminiferal calcite as a potential proxy for paleodensity (Lynch-Stieglitz  
78      et al., 1999; Billups and Schrag, 2000, LeGrande et al., 2004; Lynch-Stieglitz et al., 2007). The  
79      oxygen isotopic composition of foraminifera calcite is controlled by 1) the temperature  
80      dependence of the equilibrium fractionation during calcite precipitation and 2) the isotopic  
81      composition of seawater in which the shell grows (Urey, 1947; Shackleton, 1974). Except in  
82      areas of sea ice formation or melt, the isotopic composition of seawater ( $\delta^{18}\text{O}_{\text{sw}}$ ) is regionally  
83      related to salinity, since they are affected by processes such as evaporation, precipitation,  
84      and the water masses advection and mixing (Craig and Gordon, 1965). Therefore, both  
85      temperature and  $\delta^{18}\text{O}_{\text{sw}}$  changes that affect the foraminifera  $\delta^{18}\text{O}$  calcite ( $\delta^{18}\text{O}_{\text{c}}$ ) signal are  
86      also the processes that ultimately define the seawater density in which the foraminifera  
87      calcifies (Lynch-Stieglitz, 1999; Billups and Schrag, 2000).

88      In addition to temperature and  $\delta^{18}\text{O}_{\text{sw}}$ , the shell  $\delta^{18}\text{O}_{\text{c}}$  signal can also be potentially  
89      influenced by biological processes such as 1) photosynthesis in algal symbionts (Duplessy et  
90      al., 1970; Ravelo and Fairbanks, 1992; Spero and Lea, 1993; Spero et al., 1997) and biases  
91      due to the formation of gametogenic or ontogenetic calcite (Williams et al., 1979; Spero and  
92      Lea, 1996; Hamilton et al., 2008), 2) changes in pH and carbonate ion concentration [ $\text{CO}_3^{2-}$ ]  
93      (Spero et al., 1997; Bijma et al., 1999; Zeebe, 1999), 3) dissolution and recrystallization for  
94      shells deposited in bottom waters undersaturated in [ $\text{CO}_3^{2-}$ ] (Schrag et al., 1995), and 4)  
95      bioturbation (Waelbroeck et al., 2005). These potential processes have not been clearly  
96      demonstrated for all foraminifera species (Köhler and Mulitza, 2024) and so we do not take  
97      these effects into account. Later in this study (Sect. 3.1.2), we confirm that planktonic  
98      foraminifera  $\delta^{18}\text{O}_{\text{c}}$  is mainly related to the surface ocean density, growth season and habitat  
99      depth, with weak additional influence by biological processes.

100      Previously, Billups and Schrag (2000) used  $\delta^{18}\text{O}_{\text{c}}$  from the mixed layer planktonic  
101      foraminifera (*Globigerinoides ruber* and *Trilobatus sacculifer*) as a proxy of surface water  
102      density. They limited their study to the tropical and subtropical surface ocean.

103      In this study we investigate the use of planktonic foraminifera  $\delta^{18}\text{O}_{\text{c}}$  as a surface  
104      paleodensity proxy for the whole ocean, from low to high latitudes, using various  
105      foraminifera species: *Globigerinoides ruber* (*G. ruber*), *Trilobatus sacculifer* (*T. sacculifer*),  
106      *Globigerina bulloides* (*G. bulloides*), *Neogloboquadrina incompta* (*N. incompta*), and  
107      *Neogloboquadrina pachyderma* (*N. pachyderma*). Compared to Billups and Schrag (2000), we  
108      use extended late Holocene (LH) and last glacial maximum (LGM)  $\delta^{18}\text{O}_{\text{c}}$  databases



(Malevitch et al., 2019; Caley et al., 2014, Waelbroeck et al., 2014; Tierney et al., 2020b). We develop annual surface density calibration models using a Bayesian approach. We also use numerical climate simulations obtained with isotope enabled climate models (iLOVECLIM and ECHAM5/MPI-OM) and a foraminiferal growth module (FAME) (Roche et al., 2018) to investigate the specific seasonal dynamic and depth habitat preference of foraminifera (Roche et al., 2018; Schiebel and Hemleben 2018). We discuss the applicability and validity of the foraminifera  $\delta^{18}\text{O}$  to the past quantification of surface ocean density. We then reconstruct past surface density changes during the LGM.

117

## 118 2. Method

### 119 2.1 Planktonic foraminifera $\delta^{18}\text{O}$ databases

We compiled global foraminifera oxygen isotopic datasets from published LH and LGM measurements to allow reconstruction of past density. We used core-top and LH records of planktonic foraminifera  $\delta^{18}\text{O}$  from Malevich et al. 2019 dataset that include records from the Multiproxy Approach for the Reconstruction of the Glacial Ocean (MARGO) (Waelbroeck et al., 2005) with additional sources. This dataset consists of 2,636 observations with 1,002 for *G. ruber*, 635 for *G. bulloides*, 442 for *T. sacculifer*, 132 for *N. incompta* and 425 for *N. pachyderma* (Malevich et al., 2019). Similarly to Malevich et al. 2019, we gridded the core-top data to reduce the impact of spatial clustering by averaging samples for each species to the nearest  $1^\circ \times 1^\circ$  grid point. So doing, we obtained a total of 1,415 grid points.

For the LGM time period, records derived in part from the MARGO collection (Waelbroeck et al., 2014), with additional data from Caley et al., 2014, Tierney et al., 2020b, and from more recent studies (34 measurements). The final dataset consists of 474 observations. Chronostratigraphic quality for the LGM and LH is consistent between all the published databases, the additional observations and use the same MARGO definition (MARGO, 2009).

### 134 2.2 Ocean dataset

In order to establish and test our calibrations between foraminifera  $\delta^{18}\text{O}$  and observed surface density, we used different ocean datasets. We used the Multi Observation Global Ocean Sea Surface density product for our core-top and Late Holocene calibration models (Droghei et al., 2016; 2018). This means that we calibrated Late Holocene core-top samples against observed density fields influenced by anthropogenic climate change, an issue that affects all core-top calibrations. To test the residual of our models against sea surface temperature and salinity (SST and SSS respectively) we used WOA18 products (Locarnini et al., 2018; Zweng et al., 2018).

143

### 144 2.3 Bayesian Calibration Models and evaluation

145

Following the general approach of Malevich et al. (2019), we use Bayesian regressions to model the relationship between the calcite oxygen isotopic composition of planktonic foraminifera,  $\delta^{18}\text{O}$ , and annual mean surface density,  $\rho$ . By explicitly estimating uncertainty



in the calibration model parameters, each model produces a full posterior predictive distribution for the predictant  $\rho$ . We implement three Bayesian models—two pooling models with first- and second-degree polynomials, and a hierarchical first-degree polynomial model—using Markov chain Monte Carlo (MCMC) methods (see Kruschke, 2014; McElreath, 2018 for review).

### 2.3.1 Three Bayesian Calibration Models

#### 1. First-Degree Polynomial (Pooled), poly1\_pool:

A simple linear regression is fit to all foraminifera species combined:

$$\rho \sim N(\mu, \sigma^2), \quad \mu = \beta_0 + \beta_1 \delta^{18}O_c.$$

Weakly informative data-adaptive normal hyperpriors are used for  $\beta_0$  and  $\beta_1$ , and an exponential prior for the noise term sigma. This pooled model assumes a common relationship across all foraminifera species (see Appendix).

#### 2. Second-Degree Polynomial (Pooled), poly2\_pool:

Motivated by empirical evidence (e.g., Billups and Schrag (2000)), the second model incorporates a quadratic term:

$$\rho \sim N(\mu, \sigma^2), \quad \mu = \beta_0 + \beta_1 \delta^{18}O_c + \beta_2 (\delta^{18}O_c)^2.$$

Again, we apply weakly informative normal priors for the  $\beta_i$  parameters, ensuring flexibility while constraining the plausible range based on the observed data.

#### 3. First-Degree Polynomial (Hierarchical), poly1\_hier:

The third model recognizes that species-specific differences in calcification, depth, seasonality and vital effects can affect  $\delta^{18}O_c$  (Malevich et al., 2019). Hence, we use a hierarchical structure:

$$\rho \sim N(\mu_s, \sigma_s^2), \quad \mu_s = \beta_{s,0} + \beta_{s,1} \delta^{18}O_c.$$

where each species  $s$  has its own intercept ( $\beta_{s,0}$ ) and slope ( $\beta_{s,1}$ ). These species-level parameters are drawn from common hyperdistributions  $\nu_i$  and  $\kappa_i$  (Appendix A), ensuring partial pooling of information across species.

### 2.3.1 Model Fitting and Evaluation

All models were fitted with six independent MCMC chains of 4000 iterations each, discarding the first 2000 as burn-in. We used rank-normalized  $\hat{R}$  (Vehtari et al. 2021) to assess convergence, finding all values below 1.05. Prior and posterior predictive checks confirmed the adequacy of the models. To compare predictive performance, we computed the expected log pointwise predictive density (ELPD) via Pareto-smoothed importance sampling leave-one-out cross-validation (LOO) (Vehtari et al., 2017), which provides a principled basis for selecting the model that best characterizes the relationship between  $\delta^{18}O_c$  and  $\rho$ .

## 2.4 Isotope enabled numerical climate models

### 2.4.1 The iLOVECLIM model

The iLOVECLIM (version 1.1.3) model is a derivative of the LOVECLIM-1.2 climate model extensively described in Goosse et al. (2010). From the original model, we retain the atmospheric (ECBilt, resolution of 5.6° in latitude and longitude), oceanic (CLIO, 3x3°



189 horizontal resolution, 20 vertical layers and a free surface), vegetation (VECODE) and land  
190 surface (LBM) components and develop a complete, conservative, water isotope cycle  
191 through all cited components. A detailed description of the method used to compute the  
192 oxygen isotopes in iLOVECLIM can be found in Roche (2013) and the validation of model  
193 results can be found in Roche and Caley (2013), Caley and Roche (2013) and Extier et al.,  
194 2024.

195 We use the boundary conditions defined in/by the PMIP2 protocol to simulate the annual  
196 LGM climate (Caley et al., 2014). Details about the model simulations (LGM and pre-  
197 industrial (PI)) and validation of results for oxygen stable isotopes and temperature can be  
198 found in Caley et al. 2014.

#### 199 2.4.2 The ECHAM5/MPI-OM model

200 We also use the ECHAM5/MPIOM Earth system model, also previously named community  
201 Earth system model COSMOS. It is a fully coupled ocean–atmosphere–sea ice– land surface  
202 model (Jungclaus et al., 2006) with stable water isotope diagnostics in all relevant model  
203 components. Mass, energy, and momentum fluxes, as well as the related isotope masses of  
204 H<sub>2</sub><sup>18</sup>O and HDO, are exchanged between the atmosphere and ocean once per day. Further  
205 details about the model can be found in Werner et al., 2016.

206 We used monthly outputs of the two simulations performed for the PI and for the LGM  
207 climate as described and evaluated for oxygen stable isotopes in Werner et al., 2016.

208

#### 209 2.5 The FAME module

210 Foraminifera as Modelled Entities (FAME; Roche et al., 2018) is a foraminiferal growth  
211 module that tackles the dynamic seasonal and depth habitat of planktonic foraminifera. The  
212 module predicts the presence or absence of commonly used planktonic foraminifera and  
213 their  $\delta^{18}\text{O}$  values. It uses a very limited number of parameters, almost all derived from  
214 culture experiments (Lombard et al., 2009).

215

### 216 3. Results and discussion

#### 217 3.1 Ocean surface density from planktonic foraminifera calcite $\delta^{18}\text{O}$

218 The three Bayesian calibration models reasonably replicate core top data spread when we  
219 predict surface density (Fig. 1).

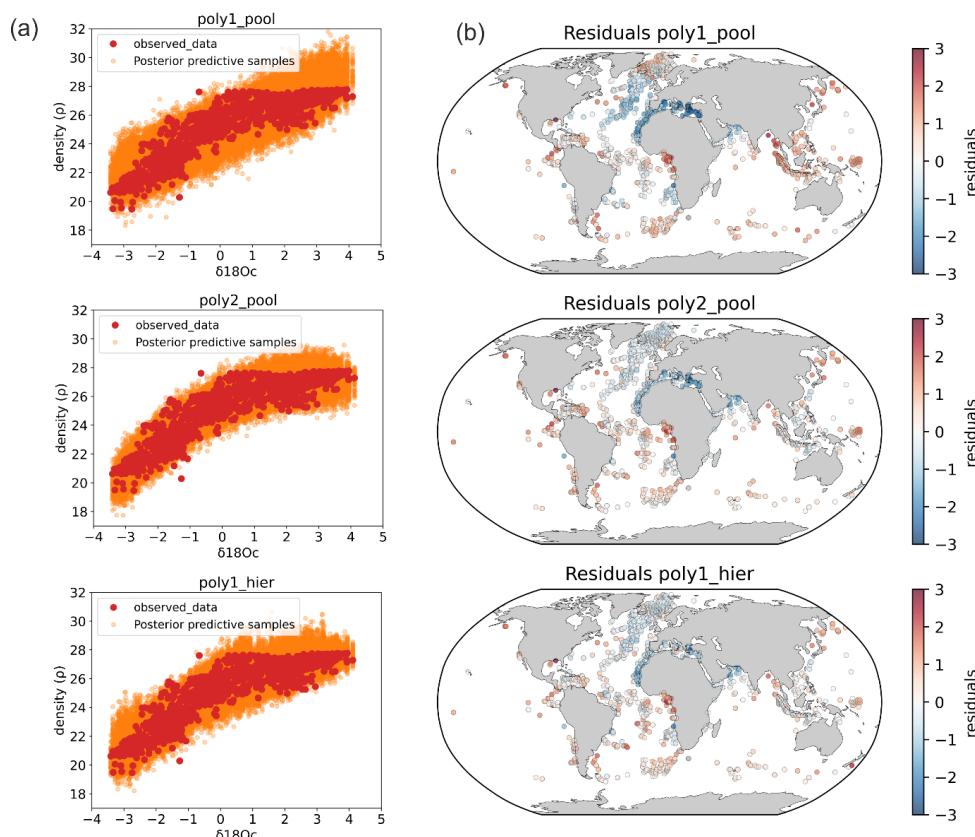
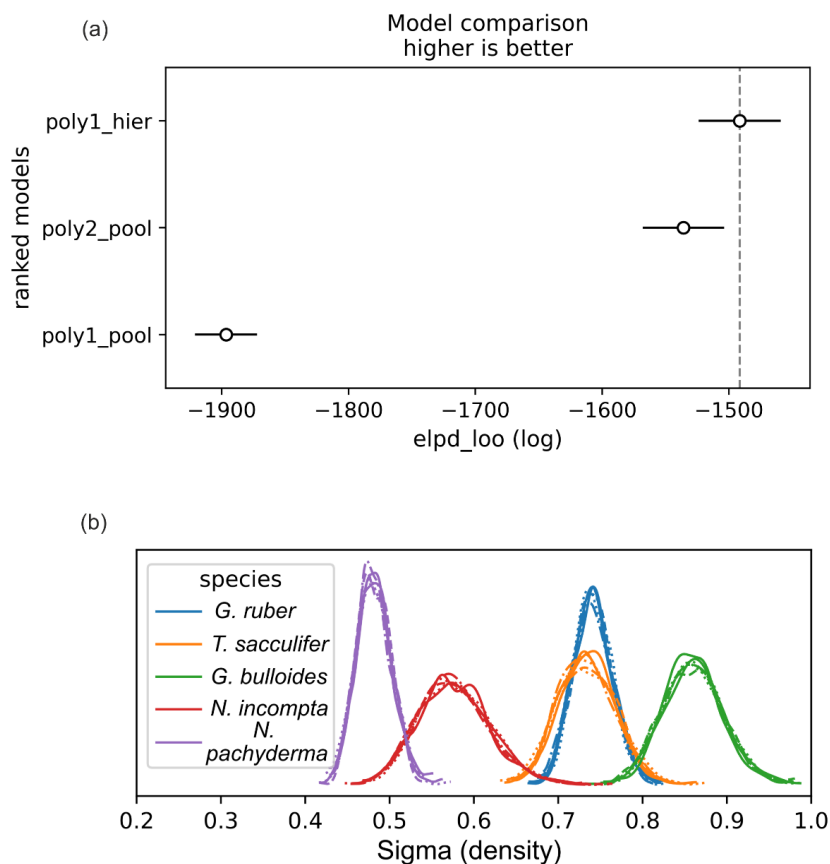


Figure 1: Bayesian calibration models. (a) The three Bayesian regression models between foraminifera  $\delta^{18}\text{Oc}$  and annual surface density and (b) associated density residuals (predicted - observed).

Compared to the Billups and Schrag (2000) study which was restricted to the 21-26 density range in tropical and subtropical regions, our models provide estimates of the density changes over the whole density range from 19 to 28 (Fig. 1). In our new calibrations, we also explicitly estimate the uncertainty in calibration model parameters (Fig. 1) using a Bayesian approach to calculate robust confidence intervals.

### 3.1.1 Model comparison and residuals

Looking at the density residual (predicted - observed) for the three models, the first model (linear pools) has the highest values of residual and the third model (hierarchical design) performs best (Fig. 1). The second model performs clearly better than the first one but less than the hierarchical design. This is supported by model evaluation using log pointwise predictive density (ELPD) (Vehtari et al., 2017) (Fig. 2). Predictive performance of the model improves when we account for species-specific differences and species-specific prediction uncertainty ( $\sigma$ ) in surface density predictions vary between foraminifera species (Fig. 2).



238

239 Figure 2: Model comparison and prediction uncertainty across species. (a) displays log  
240 pointwise predictive density (ELPD) for each model, where higher values indicate superior  
241 model fit. (b) shows species-specific prediction uncertainty (sigma density) in surface density  
242 predictions for five foraminifera species (the six independent MCMC chains are visible).  
243 Among these, *N. pachyderma* exhibits the lowest uncertainty, while *G. bulloides* shows the  
244 highest.

245

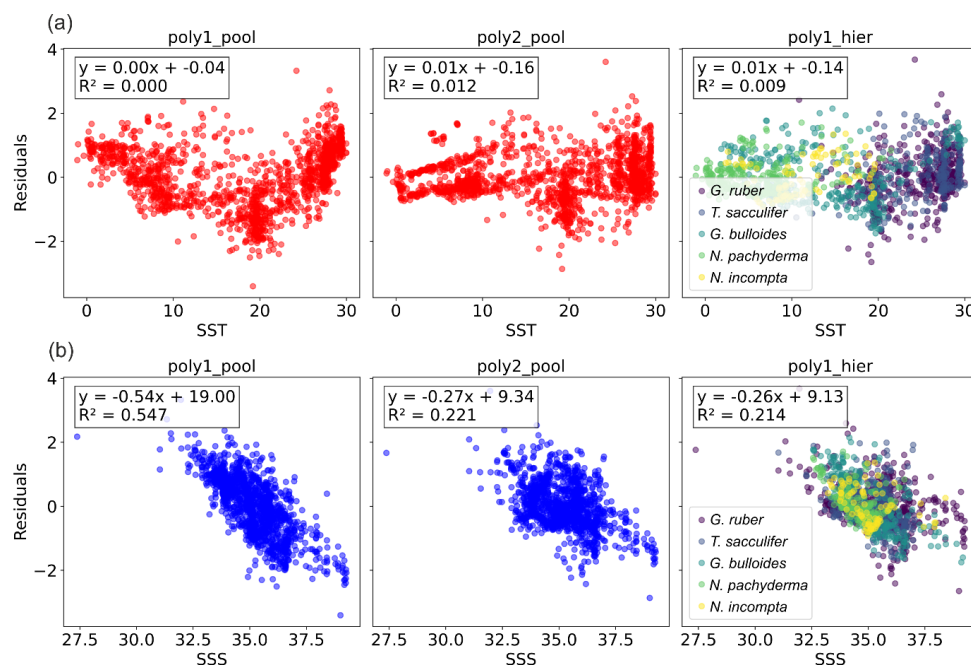
246 We still observe some residuals with the hierarchical model (Fig. 1) and so we checked the  
247 relation between SST and SSS and the residuals (Fig. 3). The residuals of the pooled linear  
248 annual calibration model exhibit a relationship with SST and a linear relationship with SSS  
249 with an observed relatively high correlation ( $R^2 = 0.55$ ). In contrast, the residuals of the  
250 hierarchical annual calibration model exhibit no correlation to SST ( $R^2 = 0$ ) and a very weak  
251 correlation to SSS ( $R^2 = 0.21$ ). So probably other factors than SST and SSS influence these  
252 residual structures that persist and some of them could indirectly be associated with  
253 gradients in SSS. Indeed, ecological factors such as seasonality and depth of life could play a  
254 role as well as secondary environmental parameters such as nutrients and light penetration.





255 This is supported by the fact that the residual of individual species (Fig. 3) have various  
256 relations with SSS of  $R^2 = 0.17$  for *G. ruber*,  $R^2 = 0.12$  for *T. sacculifer*,  $R^2 = 0.54$  for *G.*  
257 *bulloides*,  $R^2 = 0.15$  for *N. incompta*, and  $R^2 = 0.32$  for *N. pachyderma*. For example, negative  
258 residuals are observed in the Benguela, Canary, Peru and North Arabian regions (Fig. 1). All  
259 these coastal areas correspond to upwelling systems and previous work already suggested  
260 that foraminifera species could have a preference for nutrient-rich waters with high  
261 turbidity. This is particularly true for the seasonal specie *G. bulloides* (Peeters et al., 2002;  
262 Gibson et al., 2016). The  $\delta^{18}\text{O}_c$  may be strongly skewed to record cold temperatures even  
263 when accounting for seasonality and species-specific sensitivity (Malevich et al., 2019). This  
264 could explain why all three models yield lower densities than the observed annual mean  
265 densities in the upwelling zones. The negative density residuals in these upwelling regions  
266 may reflect this habitat preference (Fig. 1).

267



268

269 Figure 3: Relation between density residuals (predicted - observed) and (a) SST and (b) SSS  
270 (WOA18 products, Locarnini et al., 2018; Zweng et al., 2018) for the three Bayesian  
271 regression models.

272 We also observe high positive residual values in the Equatorial and South Atlantic Ocean, in  
273 particular on the equatorial African margin and to a lesser degree in the Equatorial East  
274 Pacific Ocean. As discussed later (Sect. 3.1.2), these positive density residuals could be  
275 related to ecological factors such as seasonality.

276 It is possible to take into account seasonality based on an estimation of foraminiferal  
277 seasonal abundance (Malevich et al. 2019), or using the FAME module. This module predicts



278 the mean  $\delta^{18}\text{O}_c$  of a foraminifera sample constituted of a number of individuals by weighting  
279 in space (depth in the water column) and time (months) the oceanic conditions by the  
280 growth rate of each individual.

281 We decided to not directly develop seasonal calibration models for several reasons. First, we  
282 want to predict annual surface density to be able to compare and evaluate numerical  
283 climate models against annual surface density. Second, including seasonal signals in  
284 foraminifera in our Bayesian models using sediment trap data (Malevich et al. 2019) or  
285 seasonality and habitat depth using FAME (that uses the temperature dependence of growth  
286 derived from culture experiments (Lombard et al., 2009)) would be a simplification that does  
287 not consider factors such as light and nutrient availability. Third, even if it could potentially  
288 improve the models for the present day calibration, although a hierarchical seasonal model  
289 does not necessary show an increase in validation performance compared to the hierarchical  
290 annual model (Malevich et al., 2019), this approach assumes that seasonality or habitat  
291 depth would not change during past periods. Results using FAME demonstrate that  
292 seasonality or habitat depth change during past periods (Roche et al., 2018). Therefore,  
293 changes in seasonality and habitat depth could introduce additional uncertainties when  
294 using a seasonal calibration model to predict past seasonal surface density. One possibility  
295 would be to use simulation results for past periods to force the FAME module and create  
296 past Bayesian calibration models between  $\delta^{18}\text{O}_c$  and surface density that would take into  
297 account ecological changes. However this would not be independent of climate models and  
298 would lead to circular reasoning if the purpose is to use reconstructed density for  
299 comparison and evaluation of past climate simulations.

300 We therefore adopt a different strategy. We use past isotope enable climate model  
301 simulations for the pre-industrial (PI) and LGM periods to force the FAME module in order to  
302 test within the “model world” if a PI Bayesian calibration (hierarchical design) between the  
303  $\delta^{18}\text{O}_c$  and annual surface ocean density is stable with time and if the changes in foraminifera  
304 growth season and habitat depth lead to additional uncertainties when applying a PI relation  
305 to past annual predictions (LGM).

306

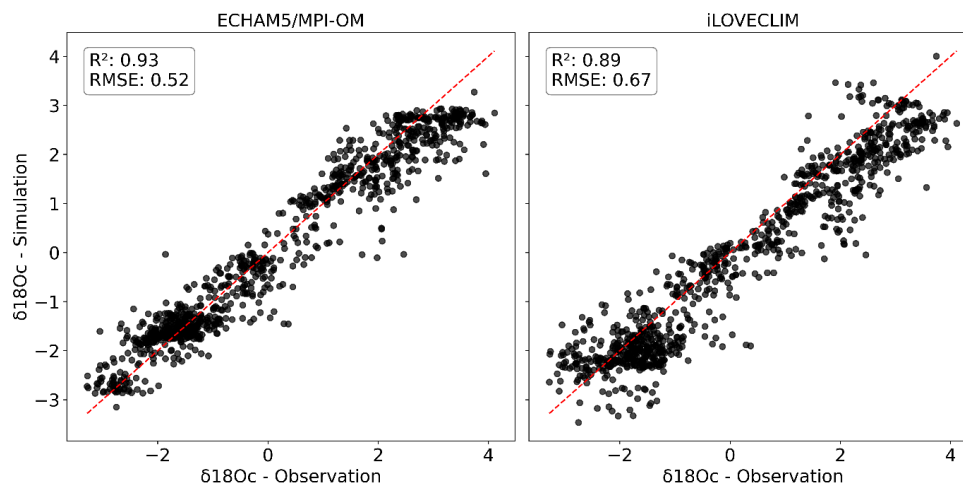
### 307 3.1.2 Testing the stability of the $\delta^{18}\text{O}_c$ -density relation during past periods

308 Because the proposed approach to reconstruct ocean surface density uses the temperature  
309 and  $\delta^{18}\text{O}_{sw}$  influence on the  $\delta^{18}\text{O}_c$  signal, we investigated the potential evolution of the  
310  $\delta^{18}\text{O}_c$ -density relationship with time before applying this approach to past density  
311 reconstructions. In particular, we investigated two questions: does the present day  $\delta^{18}\text{O}_{sw}$ -  
312 salinity relationship and its known past temporal evolution (Rohling, 2000, LeGrande and  
313 Schmidt, 2011, Caley and Roche, 2015) significantly affect the density- $\delta^{18}\text{O}_c$  relation  
314 evolution? Do ecological changes (foraminifera growth season and habitat depth)  
315 significantly affect the density- $\delta^{18}\text{O}_c$  relation evolution?

316 We use numerical climate simulations (LGM and PI) of two isotope enabled numerical  
317 climate models, iLOVECLIM and ECHAM5/MPI-OM, to address these questions. We calculate  
318 the  $\delta^{18}\text{O}_c$  signal based on the simulated  $\delta^{18}\text{O}_{sw}$  and ocean temperature for both PI and LGM



319 using the quadratic approximation of Kim and O’Neil (1997) given in Bemis et al. (1998). We  
320 use the FAME module to predict the  $\delta^{18}\text{Oc}$  values and account for foraminifera specific living  
321 habitats in the water column and along the year as described in Roche et al. (2018). A  
322 comparison of the simulated and observed core-top data  $\delta^{18}\text{Oc}$  (Fig. 4) shows high  
323 correlation ( $R^2$  of 0.93 and 0.89 for ECHAM5/MPI-OM and iLOVECLIM respectively). The  
324 slightly higher correlation with ECHAM5/MPI-OM and associated lower root mean square  
325 error (RMSE) (Fig. 4) could be related to differences in climate models but also to the fact  
326 that in the chosen configuration iLOVECLIM generated only annual  $\delta^{18}\text{Osw}$  and ocean  
327 temperature hydrographic data contrary to ECHAM5/MPI-OM that produces monthly  
328 results. Therefore, the seasonality effect is only simulated by combining FAME and  
329 ECHAM5/MPI-OM whereas the habitat depth effect is simulated in both experiments.  
330 Although climate models are not perfect, the observe high correlations demonstrate that 1)  
331 these numerical climate models can be used to address our questions regarding the stability  
332 of the  $\delta^{18}\text{Oc}$ -density relation during the past and 2) our hypothesis that planktonic  
333 foraminifera  $\delta^{18}\text{Oc}$  is mainly related to the surface ocean density, growth season and habitat  
334 depth, with weak additional influence by biological processes (Sect. 1.) is valid.



335  
336 Figure 4: comparison between simulated foraminifera  $\delta^{18}\text{Oc}$  (FAME module forced with  
337 ECHAM5/MPI-OM and iLOVECLIM climate model hydrographic data) and observed core-top  
338  $\delta^{18}\text{Oc}$  data. The 1:1 line is indicated.

339 We developed two PI bayesian calibrations (hierarchical design) between the  $\delta^{18}\text{Oc}$  and  
340 annual surface ocean density based on FAME forced by ECHAM5/MPI-OM and iLOVECLIM  
341 hydrographic data (Fig. 5a). These bayesian calibration models are comparable to the  
342 poly1\_hier bayesian calibration model of Fig. 1. We then used the LGM simulations to force  
343 FAME and produce  $\delta^{18}\text{Oc}$  LGM values comparable to those that could be measured in a  
344 marine sediment core (but in the model world). We can use these  $\delta^{18}\text{Oc}$  LGM values and the  
345 PI bayesian calibrations to predict the ocean surface density at the LGM. We can then  
346 compare the density reconstructed from the  $\delta^{18}\text{Oc}$  values to the density simulated directly at  
347 the LGM by ECHAM5/MPI-OM and iLOVECLIM. This furnish a test in the model world  
348 regarding the stability of the  $\delta^{18}\text{Oc}$ -density relation during the past.



349 Interestingly, the observed (Fig. 1) and simulated (Fig. 5b) density residuals (predicted -  
350 observed) are overall in good agreement for both PI ECHAM5/MPI-OM and iLOVECLIM  
351 experiments in terms of qualitative changes (positive or negative residuals) (Fig. 5b and Fig.  
352 1). Nonetheless, differences for some regions in terms of magnitude of the residual values  
353 exist between ECHAM5/MPI-OM and iLOVECLIM experiments. We observe high positive  
354 residuals in the Equatorial and South Atlantic Ocean in the ECHAM5/MPI-OM experiment, in  
355 particular on the equatorial African margin and in the Equatorial East Pacific Ocean. As  
356 discussed before (Sect. 3.1.1), these positive density residuals are also visible in the  
357 observations (Fig. 1b). We attribute these high positive residuals in ECHAM5/MPI-OM (Fig.  
358 5b) that better fit the observations (Fig. 1b) to a seasonality effect because seasonality is  
359 only taken into account in ECHAM5/MPI-OM experiment. Negative residuals previously  
360 discussed in upwelling regions are visible in simulated residuals but with lower magnitude in  
361 comparison to observations (Fig. 1b and 5b). This could be related to the fact that upwellings  
362 are not well simulated in the two experiments or to the role of secondary environmental  
363 parameters such as nutrients and light penetration.

364 We apply the PI annual bayesian calibration to the simulated LGM  $\delta^{18}\text{O}_c$  after a correction of  
365 1.0‰ of LGM  $\delta^{18}\text{O}_{sw}$  values (value added at LGM for the ECHAM5/MPI-OM and iLOVECLIM  
366 experiments, Caley et al., 2014, Werner et al., 2016) to account to a change of the global  
367 oceanic  $\delta^{18}\text{O}_{sw}$  signal due to the increased LGM ice sheets. This yields a prediction of the  
368 LGM surface ocean density that we can compare to the directly simulated LGM surface  
369 density in both experiments. We calculate the density residual at the LGM (density  
370 reconstructed from the  $\delta^{18}\text{O}_c$  values - density simulated directly at the LGM). Finally, we  
371 calculate the density residuals anomaly between LGM and PI as: density residuals at LGM -  
372 density residuals at PI (Fig. 5c). This allows us to investigate the additional uncertainties  
373 linked to the evolution of the density- $\delta^{18}\text{O}_c$  relation (Fig. 5c).

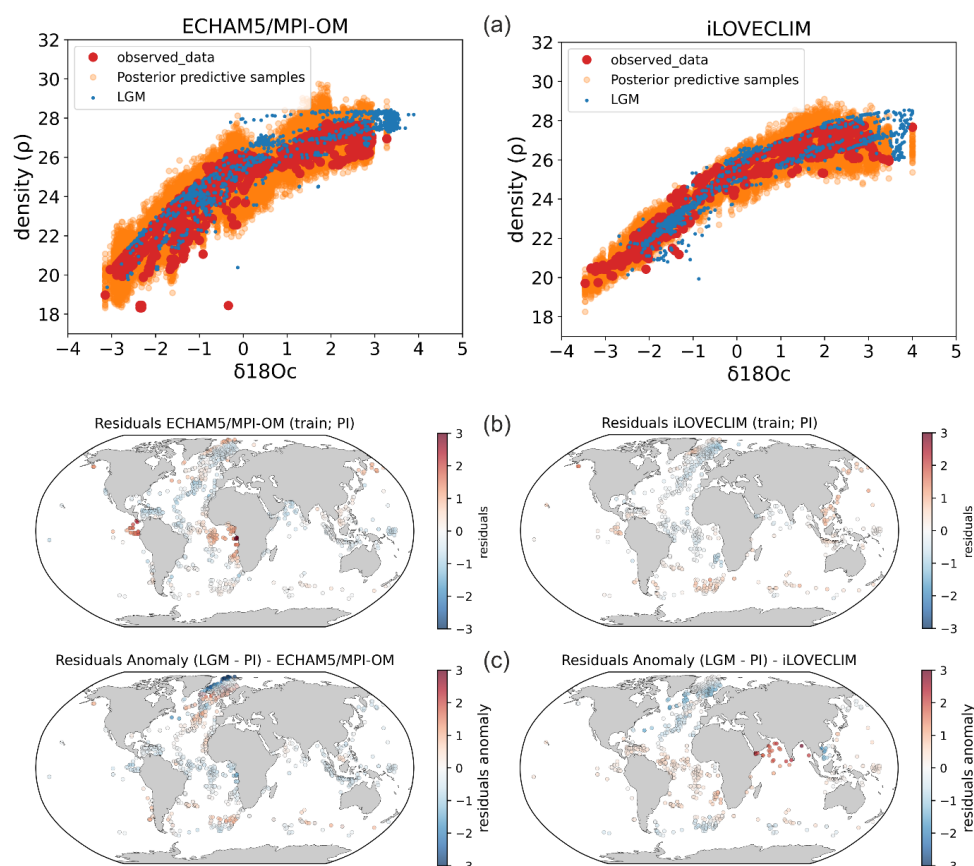


Figure 5: Stability of foraminifera  $\delta^{18}\text{Oc}$ -density relations between PI and the LGM calculated with FAME and forced by global ECHAM5/MPI-OM (left panels, Werner et al., 2016) and iLOVECLIM (right panels, Caley et al., 2014) hydrographic data. (a) PI Bayesian regression models between foraminifera  $\delta^{18}\text{Oc}$  and annual surface density. Data in the PI experiments have been selected at the same locations as observations (Fig. 1). Posterior predictive samples and LGM density prediction are visible. (b) Density residuals (predicted - observed) for the PI experiments. (c) Density residuals anomaly between LGM and PI. Results for the Mediterranean Sea have been excluded because of its difficulty to be simulated and inconsistency between the two model simulations because of their different grid resolutions. Annual mean temperature and  $\delta^{18}\text{Osw}$  were used for the iLOVECLIM experiment whereas monthly temperature and  $\delta^{18}\text{Osw}$  were used for the ECHAM5/MPI-OM experiment.

Surface density residuals anomaly (LGM - PI) are overall rather close to 0 except in the Nordic Seas region (north of  $40^\circ\text{N}$  in the Atlantic) and in the north Indian ocean for iLOVECLIM. For the North Indian Ocean in iLOVECLIM it is related to a well know bias of this climate model due to a shift of the African precipitation regions from the west to the east of the continent, leading to much less saline waters than present day observations (and unrealistically depleted  $\delta^{18}\text{Osw}$  in the North Indian Ocean (Roche and Caley, 2013). High



392 residuals anomaly in Nordic Seas region could be associated with difficulty in simulating the  
393  $\delta^{18}\text{O}_{\text{sw}}$ -salinity relation evolution related to ice-sheets and sea ice changes and/or to  
394 foraminifera ecological changes between LGM and PI.

395 To further investigate in a more quantitative way if the use of the PI bayesian calibration to  
396 predict LGM surface density introduces additional uncertainties, we compare probability  
397 distributions of surface density residuals anomaly (LGM - PI) using violin and box plots to the  
398 95% confidence interval (CI) of the PI bayesian calibration (Fig. 6). We consider each  
399 foraminifera species separately. Global results indicate for the *G. ruber* and *T. sacculifer*  
400 species that 1) the 5th to 95th percentile and interquartile range of the surface density  
401 residuals anomaly is well inside the 95% CI of the PI bayesian calibration for both  
402 ECHAM5/MPI-OM and iLOVECLIM experiment and 2) high probability and median values are  
403 close to 0 (Fig. 6a). This is not the case for *G. bulloides*, *N. incompta*, and for *N. pachyderma*.

404 When the Nordic Seas region is removed, results indicate that for all the foraminifera  
405 species, the interquartile range of the surface density residuals anomaly is well inside the  
406 95% CI of the PI bayesian calibration for both experiments (ECHAM5/MPI-OM and  
407 iLOVECLIM). High probability and median values are close to 0 (Fig. 6b). The 95% CI of the PI  
408 bayesian calibration is close to the 5th to 95th percentile range of the surface density  
409 residuals anomaly.

410

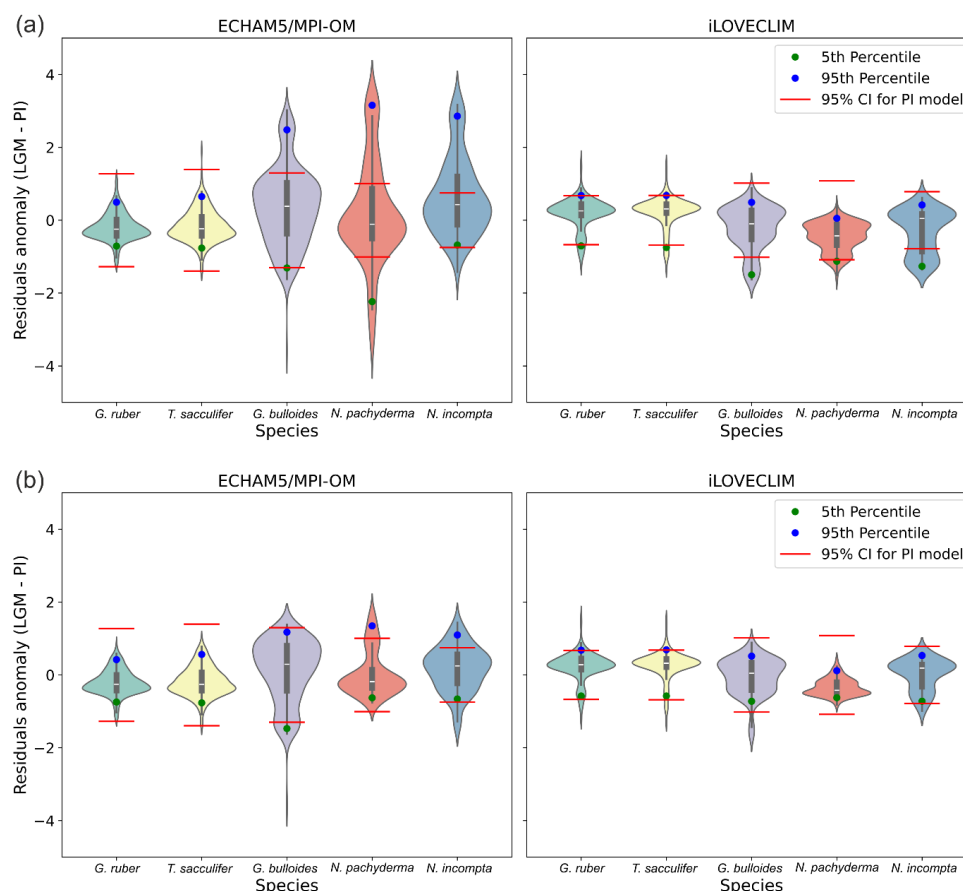


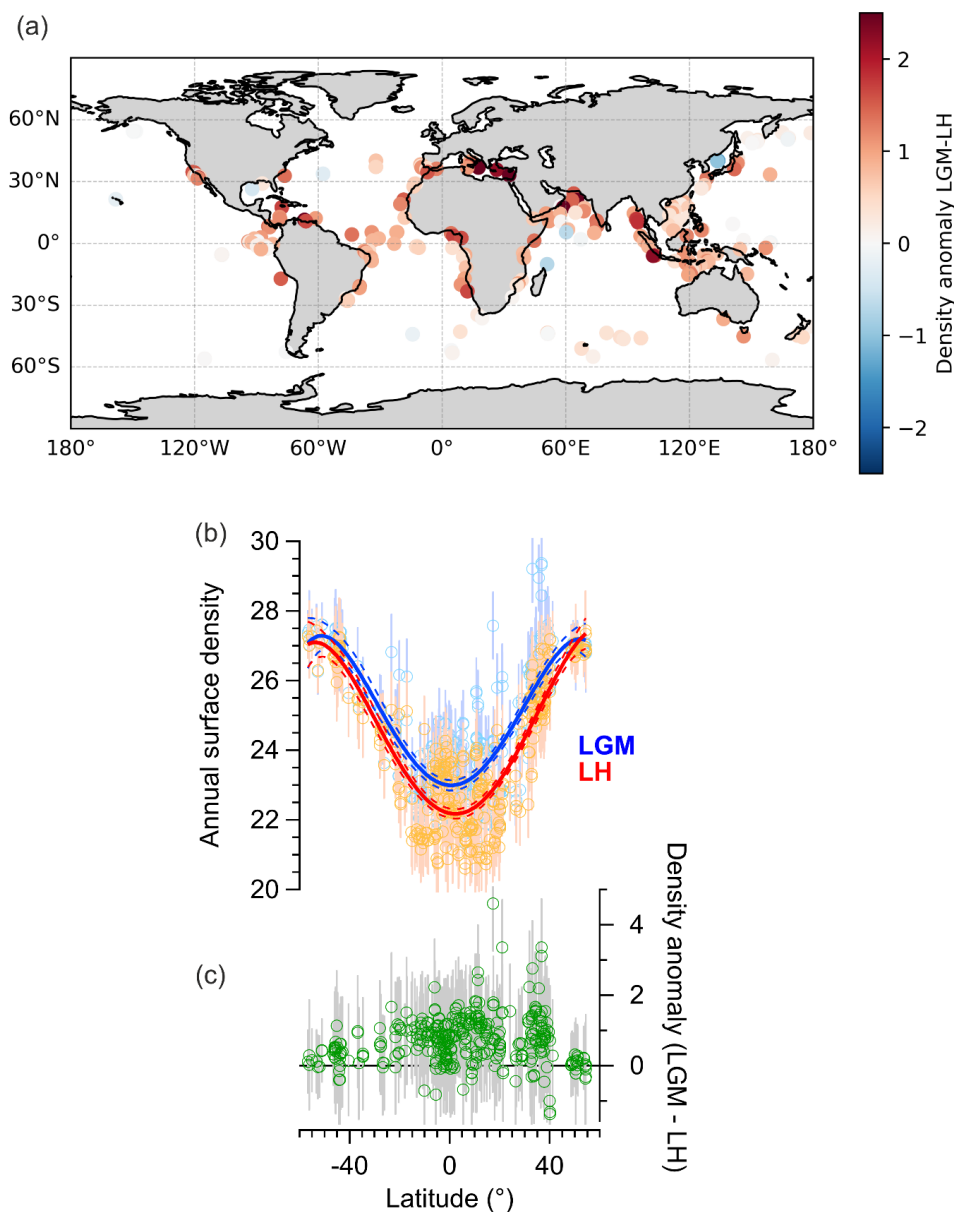
Figure 6: probability distributions of surface density residuals anomaly (LGM - PI). (a) global data and (b) without Nordic Seas (north of 40°N). North Indian Ocean data for iLOVECLIM have been removed in both cases.

We conclude based on our tests that the use of a Bayesian calibration model (hierarchical design) to predict annual surface density during past periods (with the example here of the extreme LGM climate) is valid globally within the explicitly estimated uncertainty in calibration model parameters, except for the Nordic Seas region.

### 3.2 LGM annual surface density reconstruction

We applied the poly1\_hier calibration model to the LGM and LH  $\delta^{18}\text{O}_{\text{c}}$  foraminifera database, excluding the Nordic Seas region, after subtraction of 1.05‰ from LGM  $\delta^{18}\text{O}_{\text{c}}$  values (Schrag et al., 1996; Adkins et al., 2002; Duplessy et al., 2002) in order to reconstruct LGM and LH annual surface density. The benefit of our Bayesian model is the possibility to propagate uncertainty from calibration into predictions of past climate conditions (Fig. 7).





425

426 Figure 7: reconstructions of LGM and LH annual surface ocean density from foraminifera  
 427  $\delta^{18}\text{Oc}$ . (a) Spatial distribution of the LGM - LH density anomaly. (b) Meridional gradient of  
 428 reconstructed surface annual LGM density and comparison with LH reconstructions. Error  
 429 bars for each data point represent the 80 % C.I. A polynomial fit (5th degree) and associated  
 430 95% confidence bands are shown as solid resp. dashed lines. (c) Meridional gradient of  
 431 reconstructed density anomaly (LGM - LH) and associated 80 % C.I (grey lines).

432





433 Ocean surface density increases globally during the LGM in agreement with colder SST  
434 (MARGO, 2009; Tierney et al., 2020b) and increases global salinity (Adkins et al., 2002) (Fig.  
435 7b). We also observe stronger LGM density value changes at low latitudes compared to mid  
436 latitudes (Fig. 7a and 7c). This is probably the result of the LGM cooling (MARGO, 2009;  
437 Tierney et al., 2020b) in combination with a reduction of the intensity of low latitudes  
438 hydrological cycle (Kageyama et al., 2021), whereas higher latitudes are already close to  
439 ocean density maximum. Further regional analyses of ocean surface density and comparison  
440 with numerical climate models are presented in Barathieu et al. in prep.

441

#### 442 4. Conclusions

443 We developed three Bayesian regressions to model the relationship between the calcite  
444 oxygen isotopic composition of planktonic foraminifera,  $\delta^{18}\text{O}_c$ , and annual mean surface  
445 density,  $\rho$ . This allowed us to explicitly estimate the uncertainty in calibration model  
446 parameters. We find that predictive performance of the model improves when we account  
447 for inter-species specific differences. Before applying this model to past density  
448 reconstructions, we used results of isotope enabled climate model simulations for PI and  
449 LGM time periods to force the FAME module. We then investigated the additional  
450 uncertainties that could be introduced by potential evolution of the  $\delta^{18}\text{O}_c$ -density  
451 relationship with time. It could be caused by changes in the  $\delta^{18}\text{O}_{\text{sw}}$ -salinity relationship or  
452 by foraminifera ecology. We demonstrate that additional uncertainties are weak and that  
453 our approach is valid (except for the Nordic Seas region), within propagated uncertainty  
454 from calibration into predictions of past climate conditions.

455 By applying our Bayesian regression hierarchical model to LGM and LH  $\delta^{18}\text{O}_c$  foraminifera  
456 databases we reconstruct LGM and LH annual surface density and find stronger LGM density  
457 value changes at low latitudes compared to mid latitudes. The logical next step will be to  
458 compare globally and in more detail (regional scale) our quantitative annual surface density  
459 reconstruction with densities obtained by numerical climate model simulations during the  
460 LGM. This will be used to evaluate these climate models in their ability to simulate this  
461 parameter during this extreme climatic period (Barathieu et al., in prep). The quantification  
462 of density together with the estimation of uncertainties could also be used for data  
463 assimilation approaches, allowing local paleoclimate proxy information to be used to infer  
464 global climate metrics (Tierney et al., 2020a).

465 We demonstrate that our approach is valid to quantitatively reconstruct annual surface  
466 density during one of the most extreme climates of the Quaternary period. Hence, our  
467 calibration has great potential to be applied to other past periods and to reconstruct past  
468 temporal evolution of ocean surface density downcore.

469 Finally, our calibration method to quantitatively reconstruct past ocean surface density is  
470 stable with time. A combination with existing calibration methods to reconstruct past SST  
471 could lead to a “time stable” method to quantitatively reconstruct past SSS, contrary to the  
472 use of the  $\delta^{18}\text{O}_{\text{sw}}$ -SSS approach. Before realized SSS reconstructions, further investigations  
473 and calculation of uncertainties are necessary for this potential new method. This is clearly a



474 way forward as SSS is a crucial parameter that can provide insights into hydrological cycle  
475 dynamics and its evolution.

476

477

478

479

480

481

482

483

484

485

486

487

488

489

490

491

492

493

494

495

496

497

498

499



## 500 Appendices

### 501 Appendix A. Detailed Prior Specifications

502 Below we provide the exact prior definitions and hyperparameter settings for each of the three  
503 Bayesian models. In the following,  $\rho$  denotes annual mean surface density, and  $\delta c$  represents  $\delta^{18}O_c$ .  
504 Let  $E[\rho]$  and  $\text{var}(\rho)$  be the sample mean and variance of  $\rho$ , respectively, and let  $\text{var}(\delta c)$  be the sample  
505 variance of  $\delta c$ .

#### 506 1. First-Degree Polynomial (Pooled)

507

$$\begin{aligned} \rho &\sim N(\mu, \sigma^2) \\ \mu &= \beta_0 + \beta_1 \delta c. \end{aligned}$$

508

511 We chose weakly informative and data-adaptive priors, meaning they center around observed  
512 mean/variance but are broad enough to allow for uncertainty.

513

516

$$\beta_0 \sim N(E[\rho], 2.5 \sqrt{\text{var}(\rho)}), \quad \beta_1 \sim N(0, 2.5 \sqrt{\frac{\text{var}(\rho)}{\text{var}(\delta c)}}), \quad \sigma \sim \text{Exp}(\sqrt{\text{var}(\rho)^{-1}}).$$

515

#### 517 2. Second-Degree Polynomial (Pooled)

518

$$\begin{aligned} \rho &\sim N(\mu, \sigma^2) \\ \mu &= \beta_0 + \beta_1 \delta c + \beta_2 \delta c^2. \end{aligned}$$

520

521 We set the priors to

$$\beta_i \sim N(0, 6.08^2) \quad \text{for } i \in \{0, 1, 2\}, \quad \sigma \sim \text{Exp}(\sqrt{\text{var}(\rho)^{-1}}).$$

523

524 Here, the normal priors were chosen to ensure that 90 % of the prior mass for each  $\beta_i$   
525 lies within  $[-10, 10]$ .

526

#### 527 3. First-Degree Polynomial (Hierarchical)

528

$$\begin{aligned} \rho &\sim N(\mu_s, \sigma_s^2) \\ \mu_s &= \beta_{s,0} + \beta_{s,1} \delta c \end{aligned}$$

536

529 where each species  $s$  has its own slope and intercept. These species-level  
530 parameters share hyperpriors:

531

#### 532 Species-Level Parameters

533

$$\beta_{s,i} \sim N(v_i, \kappa_i^2), \quad i \in \{0, 1\}, \quad \sigma_s \sim \text{Exp}(\lambda_s).$$

538

539

534

#### Hyperpriors



540

542

$$v_0 \sim N(E[\rho], 10), \quad v_1 \sim N(0, 10)$$

543

$$\kappa_0 \sim \text{Exp}(2.5 \sqrt{\text{var}(\rho)}), \quad \kappa_1 \sim \text{Exp}\left(2.5 \sqrt{\frac{\text{var}(\rho)}{\text{var}(\delta_c)}}\right),$$

544

$$\lambda_s^{-2} \sim \text{LogNormal}(0, 1).$$

545

541

546

547

548

549

550

551

552

553

554

555

556

557

558

559

560

561

562

563

564

565

566

567

568

569

570



571 **Code and data availability**

572 The python code for Bayesian Calibration Models will be freely available. Core top data used  
573 for this analysis are from Malevich et al. 2019 and are available at  
574 <https://agupubs.onlinelibrary.wiley.com/doi/10.1029/2019PA003576>. LGM and LH  $\delta^{18}\text{O}$   
575 dataset are available at doi:10.5194/cp-10-1939-2014-supplement for Caley et al., 2014, at  
576 <https://doi.org/10.1594/PANGAEA.894229> for Waelbroeck et al., 2014 and at  
577 <https://doi.org/10.1594/PANGAEA.920596> for Tierney et al., 2020b. The additional LGM and  
578 LH  $\delta^{18}\text{O}$  dataset will be available as a supplement.

579 **Author contributions**

580 TC and DR initially designed the study. TC developed the study. NR and TC developed  
581 Bayesian Calibration Models. MW provided ECHAM5/MPI-OM model outputs. CW furnished  
582 the new  $\delta^{18}\text{O}$  dataset. TC analysed the results with contribution and discussion of all co-  
583 authors. TC produced the figures and wrote the article with input from all co-authors.

584 **Competing interests**

585 The contact author has declared that none of the authors has any competing interests.

586 **Acknowledgements**

587 T.C. is supported by CNRS Terre & Univers. This study has been conducted using E.U.  
588 Copernicus Marine Service Information; <https://doi.org/10.48670/moi-00051>.

589 **Financial support**

590 This research was supported by the ANR HYDRATE project (grant no. ANR-21-CE01-0001) of  
591 the French Agence Nationale de la Recherche.

592

593 **References**

- 594 Adkins, J. F., McIntyre, K., and Schrag, D.: The salinity, temperature and  $\delta^{18}\text{O}$  of the glacial  
595 deep ocean, *Science* 298, 1769–1773, 2002.
- 596 Bemis, B. E., Spero, H. J., Bijma, J., and Lea, D. W.: Reevaluation of the oxygen isotopic  
597 composition of planktonic foraminifera: experimental results and revised paleotemperature  
598 equations, *Paleoceanography*, 13, 150–160, 1998.
- 599 Bijma, J., Spero, H. J., and Lea, D. W.: Reassessing foraminiferal stable isotope geochemistry:  
600 Impact of the oceanic carbonate system (experimental results), in: *Use of Proxies in*  
601 *Paleoceanography*, edited by: Fischer, G. and Wefer, G., Springer Berlin Heidelberg, 489–  
602 512, 1999.
- 603 Billups, K. and Schrag, D. P.: Surface ocean density gradients during the Last Glacial  
604 Maximum. *Paleoceanography*, 15, 110–123, 2000.



- 605 Caley, T. and Roche, D. M.:  $\delta^{18}\text{O}$  water isotope in the iLOVECLIM model (version 1.0) – Part 3:  
606 A palaeo-perspective based on present-day data–model comparison for oxygen stable  
607 isotopes in carbonates, *Geosci. Model Dev.*, 6, 1505–1516, [https://doi.org/10.5194/gmd-6-](https://doi.org/10.5194/gmd-6-1505-2013)  
608 1505-2013, 2013
- 609 Caley, T. and Roche, D. M.: Modeling water isotopologues during the last glacial: Implications  
610 for quantitative paleosalinity reconstruction, *Paleoceanography*, 30, 739–750,  
611 <https://doi.org/10.1002/2014PA002720>, 2015.
- 612 Caley, T., Roche, D. M., Waelbroeck, C., and Michel, E.: Oxygen stable isotopes during the  
613 Last Glacial Maximum climate: perspectives from data-model (iLOVECLIM) comparison, *Clim.*  
614 *Past*, 10, 1939–1955, doi:10.5194/cp-10-1939-2014, 2014.
- 615 Craig, H. and Gordon, L. I.: Deuterium and oxygen 18 variations in the ocean and the marine  
616 atmosphere, in: *Stable Isotopes in Oceanographic Studies and Paleotemperatures*, edited by:  
617 Tongiorgi, E., Lab. Geol. Nucl., Pisa, Italy, 9–130, 1965.
- 618 Droghei, R., Nardelli, B. B., and Santoleri, R.: Combining In Situ and Satellite Observations to  
619 Retrieve Salinity and Density at the Ocean Surface, *J. Atmos. Ocean. Tech.*, 33, 1211–1223,  
620 <https://doi.org/10.1175/JTECH-D-15-0194.1>, 2016.
- 621 Droghei, R., Buongiorno Nardelli, B., and Santoleri, R.: A new global sea surface salinity and  
622 density dataset from multivariate observations (1993–2016), *Frontiers in Marine Science*, 5,  
623 <https://doi.org/10.3389/fmars.2018.00084>, 2018.
- 624 Duplessy, J. C., Lalou, C., and Vinot, A. C.: Differential Isotopic Fractionation in Benthic  
625 Foraminifera and Paleotemperatures Reassessed, *Science*, 168, 250–251,  
626 <https://doi.org/10.1126/science.168.3928.250>, 1970.
- 627 Duplessy, J. C., Labeyrie, L., and Waelbroeck, C.: Constraints on the ocean oxygen isotopic  
628 enrichment between the Last Glacial Maximum and the Holocene: Paleoceanographic  
629 implications, *Quaternary Sci. Rev.*, 21, 315–330, 2002.
- 630 Extier, T., Caley, T., and Roche, D. M.: Modelling water isotopologues ( $^1\text{H}^2\text{H}^{16}\text{O}$ ,  $^1\text{H}_2^{17}\text{O}$ ) in the  
631 coupled numerical climate model iLOVECLIM (version 1.1.5), *Geosci. Model Dev.*, 17, 2117–  
632 2139, <https://doi.org/10.5194/gmd-17-2117-2024>, 2024.
- 633 Gibson, K. A., Thunell, R. C., Machain-Castillo, M. L., Fehrenbacher, J., Spero, H. J., Wejnert,  
634 K., Nava-Fernández, X., and Tappa, E. J.: Evaluating controls on planktonic foraminiferal  
635 geochemistry in the Eastern Tropical North Pacific, *Earth Planet. Sc. Lett.*, 452, 90–103, 2016.
- 636 Goosse, H., Brovkin, V., Fichet, T., Haarsma, R., Huybrechts, P., Jongma, J., Mouchet, A.,  
637 Selten, F., Barriat, P.-Y., Campin, J.-M., Deleersnijder, E., Driesschaert, E., Goelzer, H.,  
638 Janssens, I., Loutre, M.-F., Morales Maqueda, M. A., Opsteegh, T., Mathieu, P.-P., Munhoven,  
639 G., Pettersson, E. J., Renssen, H., Roche, D. M., Schaeffer, M., Tartinville, B., Timmermann,  
640 A., and Weber, S. L.: Description of the Earth system model of intermediate complexity  
641 LOVECLIM version 1.2, *Geosci. Model Dev.*, 3, 603–633, [https://doi.org/10.5194/gmd-3-603-](https://doi.org/10.5194/gmd-3-603-2010)  
642 2010, 2010.



- 643 Hamilton, C. P., Spero, H. J., Bijma, J., and Lea, D. W.: Geochemical investigation of  
644 gametogenic calcite addition in the planktonic foraminifera *Orbulina universa*, *Mar.*  
645 *Micropaleontol.*, 68, 256–267, 2008.
- 646 Jungclaus, J. H., Keenlyside, N., Botzet, M., Haak, H., Luo, J. J., Latif, M., Marotzke, J.,  
647 Mikolajewicz, U., and Roeckner, E.: Ocean circulation and tropical variability in the coupled  
648 model ECHAM5/MPI-OM, *J. Climate*, 19, 3952–3972, 2006.
- 649 Kageyama, M., Harrison, S. P., Kapsch, M.-L., Lofverstrom, M., Lora, J. M., Mikolajewicz, U.,  
650 Sherriff-Tadano, S., Vadsaria, T., Abe-Ouchi, A., Bouttes, N., Chandan, D., Gregoire, L. J.,  
651 Ivanovic, R. F., Izumi, K., LeGrande, A. N., Lhardy, F., Lohmann, G., Morozova, P. A., Ohgaito,  
652 R., Paul, A., Peltier, W. R., Poulsen, C. J., Quiquet, A., Roche, D. M., Shi, X., Tierney, J. E.,  
653 Valdes, P. J., Volodin, E., and Zhu, J.: The PMIP4 Last Glacial Maximum experiments:  
654 preliminary results and comparison with the PMIP3 simulations, *Clim. Past*, 17, 1065–1089,  
655 <https://doi.org/10.5194/cp-17-1065-2021>, 2021.
- 656 Kim, S.-T. and O’Neil, J. R.: Equilibrium and nonequilibrium oxygen isotope effects in  
657 synthetic carbonates, *Geochim. Cosmochim. Acta*, 61, 3461–3475, 1997.
- 658 Köhler, P. and Mulitza, S.: No detectable influence of the carbonate ion effect on changes in  
659 stable carbon isotope ratios ( $\delta^{13}\text{C}$ ) of shallow dwelling planktic foraminifera over the past  
660 160 kyr, *Clim. Past*, 20, 991–1015, <https://doi.org/10.5194/cp-20-991-2024>, 2024.
- 661 Kruschke, J.: Doing Bayesian data analysis: A tutorial with R, JAGS, and Stan, Academic Press,  
662 Cambridge, Massachusetts, United States, 2014.
- 663 LeGrande, A. N., Lynch-Stieglitz, J., and Farmer, E. C.: Oxygen isotopic composition of  
664 *Globorotalia truncatulinoides* as a proxy for intermediate depth density, *Paleoceanography*,  
665 19, PA4025, doi:10.1029/2004PA001045, 2004.
- 666 LeGrande, A. N. and Schmidt, G. A.: Water isotopologues as a quantitative paleosalinity  
667 proxy, *Paleoceanography*, 26, PA3225, <https://doi.org/10.1029/2010pa002043>, 2011.
- 668 Locarnini, R., Mishonov, A., Baranova, O., Boyer, T., Zweng, M., Garcia, H., Reagan, J., Seidov,  
669 D., Weathers, K., Paver, C., and Smolyar, I.: Temperature, in: *World Ocean Atlas 2018*, Vol. 1,  
670 edited by: Mishonov, A., NOAA Atlas NESDIS 81, 2018.
- 671 Lombard, F., Labeyrie, L., Michel, E., Spero, H. J., and Lea, D. W.: Modelling the temperature  
672 dependent growth rates of planktic foraminifera, *Mar. Micropaleontol.*, 70, 1–7, 2009.
- 673 Lynch-Stieglitz, J., Curry, W. B., and Slowey, N.: A Geostrophic Transport Estimate for the  
674 Florida Current from the Oxygen Isotope Composition of Benthic Foraminifera,  
675 *Paleoceanography*, 14, 360–373, doi:10.1029/1999pa900001, 1999.
- 676 Lynch-Stieglitz, J., Adkins, J. F., Curry, W. B., Dokken, T., Hall, I. R., Herguera, J. C., Hirschi, J.  
677 J.-M., Ivanova, E. V., Kissel, C., Marchal, O., Marchitto, T. M., McCave, I. N., McManus, J. F.,  
678 Mulitza, S., Ninnemann, U., Peeters, F., Yu, E.-F., and Zahn, R.: Atlantic Meridional  
679 Overturning Circulation During the Last Glacial Maximum, *Science*, 316, 66,  
680 <https://doi.org/10.1126/science.1137127>, 2007.



- 681 Malevich, S. B., Vetter, L., and Tierney, J. E.: Global core top calibration of  $\delta^{18}\text{O}$  in planktic  
682 foraminifera to sea surface temperature, *Paleoceanogr. Paleoclimatol.*, 34, 1292–1315,  
683 2019.
- 684 MARGO Project Members: Constraints on the magnitude and patterns of ocean cooling at  
685 the Last Glacial Maximum, *Nat. Geosci.*, 2, 127–132, <https://doi.org/10.1038/NGEO411>,  
686 2009.
- 687 McElreath, R.: Statistical rethinking: A bayesian course with examples in R and Stan,  
688 Chapman and Hall/CRC, <https://doi.org/10.1201/9781315372495>, 2018.
- 689 Peeters, F. J. C., Brummer, G.-J. A., and Ganssen, G.: The effect of upwelling on the  
690 distribution and stable isotope composition of *Globigerina bulloides* and *Globigerinoides*  
691 *ruber* (planktic foraminifera) in modern surface waters of the NW Arabian Sea, *Global*  
692 *Planet. Change*, 34(3–4), 269–291, 2002.
- 693 Ravelo, A. C. and Fairbanks, R. G.: Oxygen Isotopic Composition of Multiple Species of  
694 Planktonic Foraminifera: Records of the Modern Photoc Zone Temperature Gradient,  
695 *Paleoceanography*, 7, 815–831, 1992.
- 696 Roche, D. M.:  $\delta^{18}\text{O}$  water isotope in the iLOVECLIM model (version 1.0) – Part 1:  
697 Implementation and verification, *Geosci. Model Dev.*, 6, 1481–1491,  
698 <https://doi.org/10.5194/gmd-6-1481-2013>, 2013.
- 699 Roche, D. M. and Caley, T.:  $\delta^{18}\text{O}$  water isotope in the iLOVECLIM model (version 1.0) – Part 2:  
700 Evaluation of model results against observed  $\delta^{18}\text{O}$  in water samples, *Geosci. Model Dev.*, 6,  
701 1493–1504, <https://doi.org/10.5194/gmd-6-1493-2013>, 2013.
- 702 Roche, D. M., Waelbroeck, C., Metcalfe, B., and Caley, T.: FAME (v1.0): a simple module to  
703 simulate the effect of planktonic foraminifer species-specific habitat on their oxygen isotopic  
704 content, *Geosci. Model Dev.*, 11, 3587–3603, <https://doi.org/10.5194/gmd-11-3587-2018>,  
705 2018.
- 706 Rohling, E. J.: Paleosalinity: confidence limits and future applications, *Mar. Geol.*, 163, 1–11,  
707 2000.
- 708 Schiebel, R. and Hemleben, C.: Planktic Foraminifers in the Modern Ocean, Springer-Verlag,  
709 Berlin Heidelberg, 358 pp., 2017.
- 710 Schrag, D. P., DePaolo, D. J., and Richter, F. M.: Reconstructing past sea surface  
711 temperatures: Correcting for diagenesis of bulk marine carbonate, *Geochim. Cosmochim.*  
712 *Acta*, 59, 2265–2278, [https://doi.org/10.1016/0016-7037\(95\)00105-9](https://doi.org/10.1016/0016-7037(95)00105-9), 1995.
- 713 Schrag, D. P., Hampt, G., and Murray, D. W.: Pore fluid constraints on the temperature and  
714 oxygen isotopic composition of the glacial ocean, *Science*, 272, 1930–1932, 1996.
- 715 Shackleton, N. J.: Attainment of isotopic equilibrium between ocean water and the  
716 benthonic foraminifera *Uvigerina*: Isotopic changes in the ocean during the last glacial,  
717 *Colloq. Int. du Cent. Natl. la Rech. Sci.*, 219, 203–210, 1974.





- 1718 Spero, H. J. and Lea, D. W.: Intraspecific stable isotope variability in the planktic foraminifera  
1719 Globigerinoides sacculifer: Results from laboratory experiments, Mar. Micropaleontol., 22,  
1720 221–234, 1993.
- 1721 Spero, H. J. and Lea, D. W.: Experimental determination of stable isotope variability in  
1722 Globigerina bulloides: Implications for paleoceanographic reconstruction, Mar.  
1723 Micropaleontol., 28, 231–246, doi:10.1016/0377-8398(96)00003-5, 1996.
- 1724 Spero, H. J., Bijma, J., Lea, D. W., and Bemis, B. E.: Effect of seawater carbonate  
1725 concentration on foraminiferal carbon and oxygen isotopes, Nature, 390, 497–500, 1997.
- 1726 Tierney, J. E., Poulsen, C. J., Montañez, I. P., Bhattacharya, T., Feng, R., Ford, H. L., Hönsch,  
1727 B., Inglis, G. N., Petersen, S. V., Sagoo, N., and Tabor, C. R.: Past climates inform our future,  
1728 Science, 370, eaay3701, <https://doi.org/10.1126/science.aay3701>, 2020a.
- 1729 Tierney, J. E., Zhu, J., King, J., Malevich, S. B., Hakim, G. J., and Poulsen, C. J.: Glacial cooling  
1730 and climate sensitivity revisited, Nature, 584, 569–573, 2020b.
- 1731 Urey, H. C.: The thermodynamic properties of isotopic substances, J. Chem. Soc., 562–581,  
1732 <https://doi.org/10.1039/JR9470000562>, 1947.
- 1733 Vehtari, A., Gelman, A., and Gabry, J.: Practical Bayesian model evaluation using leave-one-  
1734 out cross-validation and WAIC, Stat. Comput., 27, 1413–1432,  
1735 <https://doi.org/10.1007/s11222-016-9696-4>, 2017.
- 1736 Vehtari, A., Gelman, A., Simpson, D., Carpenter, B., and Bürkner, P.-C.: Rank-Normalization,  
1737 Folding, and Localization: An Improved  $\hat{R}$  for Assessing Convergence of MCMC (with  
1738 Discussion), Bayesian Anal., 16, 667–718, <https://doi.org/10.1214/20-BA1221>, 2021.
- 1739 Waelbroeck, C., Mulitza, S., Spero, H., Dokken, T., Kiefer, T., and Cortijo, E.: A global  
1740 compilation of Late Holocene planktic foraminiferal  $\delta^{18}\text{O}$ : Relationship between surface  
1741 water temperature and  $\delta^{18}\text{O}$ , Quaternary Sci. Rev. 24, 853–878, 2005.
- 1742 Waelbroeck, C., Kiefer, T., Dokken, T., Chen, M. T., Spero, H. J., Jung, S., Weinelt, M., Kucera,  
1743 M., and Paul, A.: Constraints on surface seawater oxygen isotope change between the Last  
1744 Glacial Maximum and the Late Holocene, Quaternary Sci. Rev., 105, 102–111,  
1745 <https://doi.org/10.1016/j.quascirev.2014.09.020>, 2014.
- 1746 Werner, M., Haese, B., Xu, X., Zhang, X., Butzin, M., and Lohmann, G.: Glacial–interglacial  
1747 changes in  $\text{H}_2^{18}\text{O}$ , HDO and deuterium excess – results from the fully coupled ECHAM5/MPI-  
1748 OM Earth system model, Geosci. Model Dev., 9, 647–670, [https://doi.org/10.5194/gmd-9-](https://doi.org/10.5194/gmd-9-647-2016)  
1749 647-2016, 2016.
- 1750 Williams, D. F., Bé, A. W., and Fairbanks, R. G.: Seasonal oxygen isotopic variations in living  
1751 planktonic foraminifera off Bermuda, Science, 206, 447–449, 1979.
- 1752 Zeebe, R. E.: An explanation of the effect of seawater carbonate concentration on  
1753 foraminiferal oxygen isotopes, Geochim. Cosmochim. Acta, 63, 2001–2007,  
1754 [https://doi.org/10.1016/S0016-7037\(99\)00091-5](https://doi.org/10.1016/S0016-7037(99)00091-5), 1999.



755    Zweng, M., Reagan, J., Seidov, D., Boyer, T., Locarnini, R., Garcia, H., Mishonov, A., Baranova,  
756    O., Weathers, K., Paver, C., and Smolyar, I.: Salinity, in: World Ocean Atlas 2018, Vol. 2,  
757    edited by: Mishonov, A., NOAA Atlas NESDIS 82, 2018.